Engineering Analysis with Boundary Elements 103 (2019) 80–93

Contents lists available at ScienceDirect

Engineering Analysis with Boundary Elements

journal homepage: www.elsevier.com/locate/enganabound

A binary-tree subdivision method for evaluation of singular integrals in 3D BEM

Jianming Zhang[a,*], Chuanming Ju[a], Eduardo Divo[b], Yudong Zhong[a], Baotao Chi[a]

[a] State Key Laboratory of Advanced Design and Manufacturing for Vehicle Body, College of Mechanical and Vehicle Engineering, Hunan University, Changsha 410082, China

[b] Department of Mechanical Engineering, College of Engineering, Embry-Riddle Aeronautical University, Daytona Beach, FL, USA

ARTICLE INFO

Keywords:
Singular integrals
Element subdivision
Binary-tree

ABSTRACT

A binary-tree subdivision method for evaluation of singular integrals in three-dimensional (3D) boundary element method (BEM) is presented in this paper. Element subdivision is one of the most widely used methods for evaluating singular integrals. In the traditional subdivision method, the sub-elements are obtained by simply connecting the source point with each vertex of the element and thus the integral accuracy is easily affected by the shape of the element and the location of the source point. The Spherical Element Subdivision Method can be used to evaluate singular integrals accurately and efficiently for cases of arbitrary element shape and arbitrary location of the source point. However, this method does not guarantee appropriate element subdivision. Therefore, in this paper, we present a new element subdivision method based on a binary-tree approach. This subdivision algorithm is more convenient to implement and can guarantee the convergence of the iterative subdivision based on a given terminating condition. Numerical examples for planar and curved surface elements with various relative locations of the source point are presented. The results demonstrate that the binary-tree subdivision method can provide much better accuracy and efficiency with fewer Gaussian points than the conventional subdivision method.

1. Introduction

Accurate and efficient evaluation of singular integrals has long been an issue of major concern in boundary element method (BEM) implementations [1–19]. Element subdivision is one of the most widely used methods for singular integration. In the conventional subdivision method, the sub-elements which are also called patches, are obtained by simply connecting the singular point with each vertex of the element [20]. This method is performed in the local coordinate system of the element rather than in the physical coordinate system. As such, the method may produce “badly-shaped” patches in cases where the element is distorted or the element is highly irregular, as it is the case for elements obtained by conventional mesh generation techniques. An example of slender elements is shown in Fig. 1.

An illustration of the patches obtained by the conventional subdivision method is shown in Fig. 2(a)–(c) corresponding to different locations of the source point. Table 1 shows that the accuracy of Gaussian integration with the 1/r kernel on these patches is unacceptable, even suggesting very little improvement with a significant increase in the number of Gaussian points. This example reveals that much attention should be paid to the subdivision scheme, particularly in cases of irregularly-shaped elements.

Zhang and co-workers [1,2,6] proposed the Spherical Subdivision Method (SSM) to overcome the issues with the conventional subdivision method. In the SSM the elements are not subdivided in the local coordinate system but instead in the physical coordinate system. An element is subdivided into a number of patches through a sequence of spheres with decreasing radius and the obtained patches are automatically refined as they approach the source point. Each patch is then appropriate in shape and size for standard Gaussian quadrature integration. Divo and Kassab [21,22] proposed a technique to subdivide singular quadrilateral elements in successive quadrilaterals surrounding four triangular regions around the singularity further transformed into local polar coordinates for numerical integration. The successive subdivision followed a threshold and yielded accurate results. However, this technique as well as the SSM and other empirical methods such as the mesh generation Advancing Front Method (AFM), do not guarantee convergence or successful element subdivision. Thus a Binary-Tree Subdivision Method (BTSM) is proposed in this paper. The proposed BTSM splits an element into two patches at each step, and continues the splitting process recursively until meeting a given terminating criterion. This subdivision algorithm is less cumbersome to implement than other subdivision methods and can guarantee the convergence of the iterative subdivision based on the given terminating criteria [23–25]. The patches that intersect with the

* Corresponding author.
E-mail address: zhangjm@hnu.edu.cn (J. Zhang).

https://doi.org/10.1016/j.enganabound.2019.03.007
Received 4 November 2018; Received in revised form 24 February 2019; Accepted 5 March 2019
Available online 16 March 2019

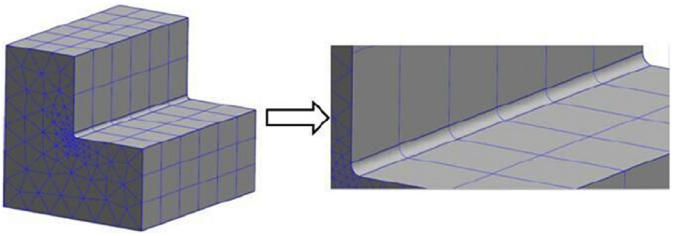

Fig. 1. Slender curved elements on the fillet face.

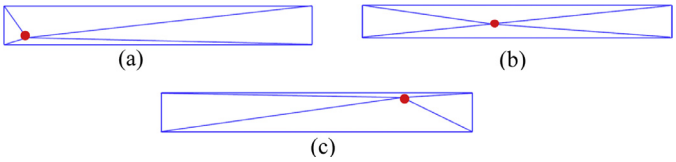

Fig. 2. Patches obtained by the conventional subdivision method.

Table 1
Integral accuracy obtained by conventional subdivision method.

Gaussian points number			Relative error		
Patches (A)	Patches (B)	Patches (C)	Patches (A)	Patches (B)	Patches (C)
116	80	154	3.77e−02	3.43e−02	3.96e−02
189	146	251	2.60e−02	3.08e−02	2.13e−02
322	248	432	1.27e−02	2.20e−02	1.82e−02
489	374	642	1.16e−02	1.97e−02	1.63e−02
633	456	835	4.43e−03	1.36e−02	1.14e−03
860	629	1107	1.53e−03	3.30e−03	1.00e−03

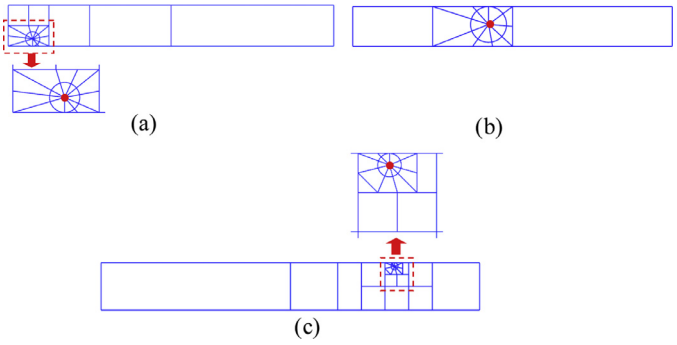

Fig. 3. Sample patches obtained by the BTSM.

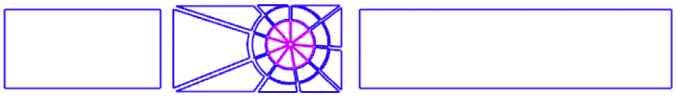

Fig. 4. Further BTSM subdivision of singular patches.

sphere centered at the source point are set to be invalid, and thus a cavity is formed. New patches will be generated along the radial direction of the sphere to fill this cavity, resulting in regularly-shaped patches. Some sample BTSM subdivision results are shown in Fig. 3(a)–(c).

In addition, the singular patches shown in Fig. 3(b) can be further subdivided by the BTSM as shown in the Fig. 4.

The rest of the paper is organized as follows: Section 2 introduces the details of the Binary-Tree Subdivision Method (BTSM); Section 3 describes the integration over the singular patches using a four-node serendipity element; Section 4 provides a comprehensive set of numerical examples; and Section 5 drafts the conclusions.

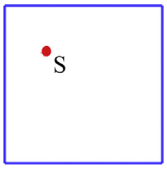

Fig. 5. Sample singular element showing location of source point S.

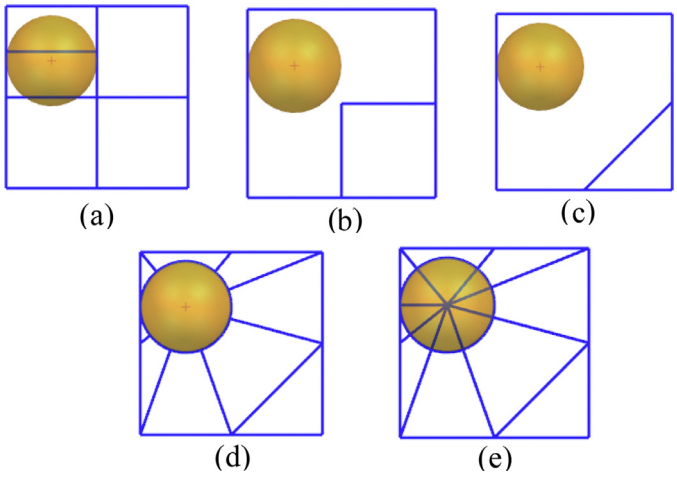

Fig. 6. The subdivision process of the BTSM.

2. The binary-tree subdivision method (BTSM)

2.1. The algorithm

To illustrate the BTSM, the singular element shown in Fig. 5 will be used as an example. The subdivision process of the BTSM is graphically illustrated in Fig. 6.

Fig. 6(a) shows the initial results of the BTSM subdivision process; this process is further described in detail in Section 2.2. Fig. 6(b) and (c) shows the formation of the cavity and its interaction with the patches. The details of forming this cavity are described in Section 2.3. Fig. 6(d) and (e) shows the process of completing the patches and filling the cavity with radial patches. The radial patches are the sub-elements whose side edges are along the radial direction of the final circular cavity whose radius is the nearest distance between the source point and the edges of the element.

2.2. Initial subdivision

The initial subdivision of binary-tree method is similar to the quadtree decomposition [23–29] in which each parent is recursively divided into four children. In the BTSM, the singular boundary element is subdivided into two sub-elements or patches. Each patch is then examined to determine if it is to be subdivided based on a specific subdivision criterion. If it is to be subdivided, two new patches are created from this patch using the same approach. The process continues until the subdivision criterion for all remaining patches is not met. The subdivision criterion ensures that those patches in close proximity to the source point or which contain the source point are subjected to subdivision while those far from the source point are not subdivided. The details of the subdivision criterion and process are described below (Fig. 7).

In Fig. 8, S is the source point, C is the center of a circle circumscribed on an element patch, R is the radius of the circumscribed circle, and L is the distance from C to S. If the ratio L/R is smaller than a prescribed value, the patch is assumed to be close enough to the source point to warrant subdivision into two additional patches. Conversely, if the ratio L/R is larger than that prescribed value, the patch is not subjected to further subdivision. It is worth noting that if R is smaller than the radius

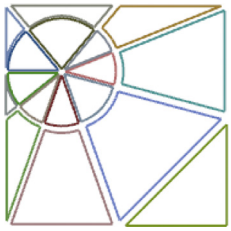

Fig. 7. The final subdivision result of the Binary-tree subdivision method.

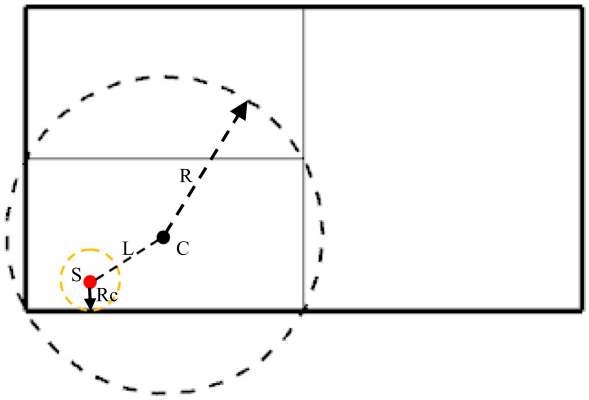

Fig. 8. Distance-based element subdivision criterion.

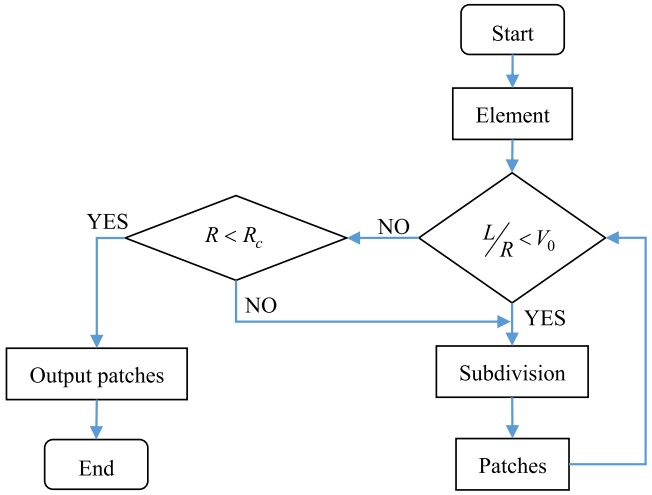

Fig. 9. Flow diagram of initial subdivision algorithm.

of the cavity R_c around the source point, the subdivision of the patch will also stop. The subdivision is further described in the flow diagram shown in Fig. 9.

2.3. The formation of the cavity and the radial patches

The radius of the cavity R_c is established as the distance between the source point and the nearest edge. If the distance between any given patch vertex and the source point is less than R_c then this vertex is inside the cavity and the patch is removed from the subdivision. If the distance between any given patch edge and the source point is less than R_c then the patch is also removed from the subdivision. This process is shown in Fig. 6(a)–(c).

The process of creating the radial patches involves two steps: the first step generates external radial patches between every vertex from the initial subdivision and the cavity by projecting in the radial direction from the source point, as shown in Fig. 6(d); while the second step generates

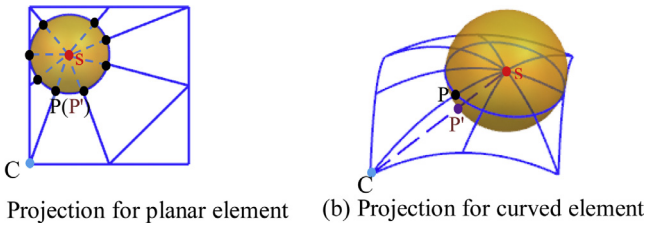

Fig. 10. Projection points corresponding to the points on the cavity.

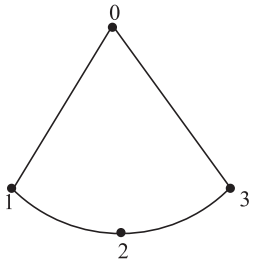

Fig. 11. Four-node serendipity triangular patch.

internal radial patches within the cavity using these projection points, as shown in Fig. 6(e). For planar elements, the determination of intersection points with the cavity through radial projection is straightforward as shown in Fig. 10(a); however, for curved elements, the intersection points are found by depicting the cavity as a sphere and following a process that starts with a linear projection between the source point and each vertex to find point P' and iteratively moving this point along the perimeter of the sphere until it finds the element surface at the actual intersection point P. This process is shown in Fig. 10(b) where the point S corresponds to the center of the cavity, the point C is a subdivision vertex on the element, the linear connection between point S and point C and its intersection with the sphere results in point P', and its iterative movement along the sphere surface until it reaches the element surface is point P.

After generating the outer radial patches, the inner radial patches are generated by connecting the projection points with the source point, as shown in Fig. 6(e) and Fig. 10(a), (b).

3. Four-node serendipity triangular patch

After the binary tree subdivision of a boundary element, four-node serendipity triangular patches are obtained. These serendipity patches, proposed by Zhang and co-workers [6], require fewer sample points to obtain higher integration accuracy. A typical serendipity triangular patch is as shown in Fig. 11 where the distance $\overline{01}$ and the distance $\overline{03}$ are equal to the radius of the cavity.

A local coordinate transformation is used to eliminate the singularity at point 0. This is shown in Fig. 12.

Consider the following integral over the patch surface S:

$$I(\xi) = \int_S \frac{f(x,\xi)}{|x-\xi|}\phi(x)dS(x) \tag{1}$$

Here ξ refers to the singular point (x_0,y_0), $\boldsymbol{x}$ refers to a field point (x, y), $|x-\xi|$ represents the distance between a field point and the singular point hence weakly singular at point 0, $f(x, \xi)$ is a well-behaved function, and $\varphi(x)$ is a shape function.

For this patch, a coordinate transformation in terms of a local coordinate ρ and a local coordinate θ can be written as:

$$\begin{cases} x = x_0 + (x_a - x_0)\rho \\ y = y_0 + (y_a - y_0)\rho \end{cases} \quad \because \quad \rho \in [0,1] \tag{2}$$

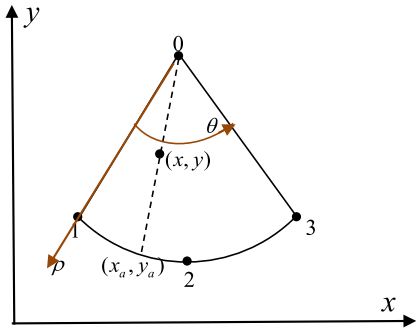

Fig. 12. The coordinate transformation of serendipity triangular patch.

Such that the field points on the arch $\overset{\frown}{123}$ are interpolated as:

$$\begin{cases} x_a = N_1(\theta)x_1 + N_2(\theta)x_2 + N_3(\theta)x_3 \\ y_a = N_1(\theta)y_1 + N_2(\theta)y_2 + N_3(\theta)y_3 \end{cases} \quad \because \quad \theta \in [-1, 1] \tag{3}$$

where $N_1(\theta)$, $N_2(\theta)$, and $N_3(\theta)$ are quadratic shape functions to approximate the arch $\overset{\frown}{123}$ as a parabola. Then the integral $I(\xi)$ can be written as:

$$I(\xi) = \int_{-1}^{1}\int_{0}^{1} \frac{f(x,\xi)}{|x-\xi|}\phi(x)J(\rho,\theta)d\rho d\theta \tag{4}$$

where $J(\rho, \theta)$ is the Jacobian of the transformation from the x–y system to the ρ–θ system, such that:

$$J(\rho,\theta) = \rho\left[\left(x_a - x_0\right)\frac{\partial y_a}{\partial \theta} - \left(y_a - y_0\right)\frac{\partial x_a}{\partial \theta}\right]. \tag{5}$$

Note that the weak singularity in the integral $I(\xi)$ is removed by the implementation of this transformation as the Jacobian in Eq. (5) introduces the local coordinate ρ in the numerator. It can also be noted that this new coordinate system transformation is much simpler to implement than the conventional polar coordinate system in [30], as the local coordinates ρ and θ are automatically constrained to the intervals [0, 1]and [−1, 1]respectively, rendering the four-node serendipity triangular patch computationally more efficient [6].

4. Numerical examples

To verify the accuracy and efficiency of the BTSM several computational experiments are implemented to compare its accuracy against exact solutions and that of the conventional subdivision method (CSM) in [30], for planar and curved elements. For the purpose of error estimation, a relative error is defined as follows:

$$Error = \left|\frac{I_n - I_e}{I_e}\right| \tag{6}$$

where I_n and I_e are the numerical approximation and exact solution of the integral, respectively. For all cases, the following weakly singular integral is considered:

$$I(\xi) = \int_S \frac{1}{|x-\xi|} dS(x) \tag{7}$$

In all numerical examples the non-singular quadrilateral and triangular patches that are evaluated by standard Gaussian and Hammer quadrature integration respectively. The number of Gaussian points m is determined by the following relation, see [28,29]:

$$m = -\frac{1}{10}\ln\left(\frac{e}{2}\right)\sqrt{\frac{2}{3}p + \frac{2}{5}}\left[\left(\frac{8L}{3R}\right)^{\frac{3}{4}} + 1\right] \tag{8}$$

where p represents the order of the singularity ($p = 1, 2, 3$), $e$denotes the error tolerance, L is the length of the patch in the integral direction, and R is the minimum distance from the source point to the boundary element.

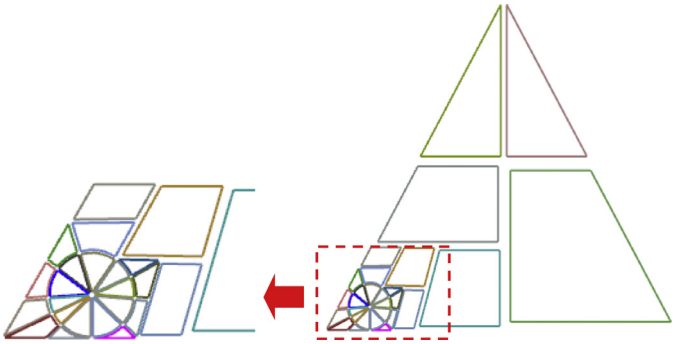

Fig. 13. Subdivision of regular triangular element with BTSM with source point at (0.09, 0.07).

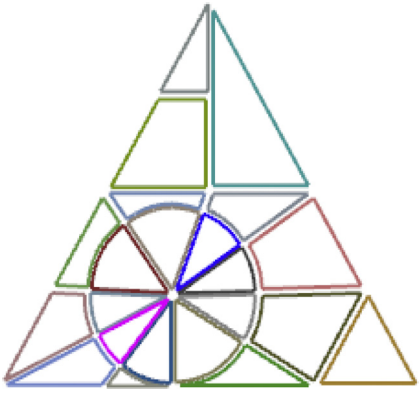

Fig. 14. Subdivision of regular triangular element with BTSM with source point at (0.295, 0.26).

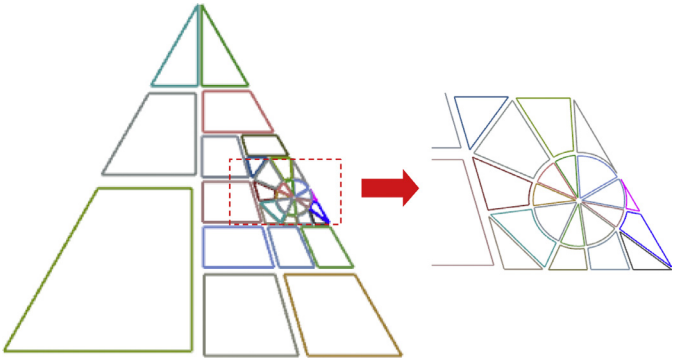

Fig. 15. Subdivision of regular triangular element with BTSM with source point at (0.5, 0.45).

4.1. Singular integration on planar element examples

For demonstration purposes, planar elements with regular, slender, and obtuse triangular shapes are included in the following set of numerical experiments. The coordinates of the vertices of the regular triangle element are (0,0,0), (10,0,0), (5,8.6,0) in the physical coordinate system, while the coordinates of the vertices of the slender triangle element are (0,0,0), (6,0,0), (3,15,0), and coordinates of the vertices of the obtuse triangle element are (0,0,0), (10,0,0), (20,10,0). Also, planar quadrilateral elements with regular, slender, and irregular shapes are included. The coordinates of the vertices of the regular quadrilateral element are (0,0,0), (10,0,0), (10,10,0), (0,10,0) in the physical coordinate system, while the coordinates of the vertices of the slender quadrilateral element are (0,0,0), (20,0,0), (20,2.5,0), (0,2.5,0), and the coordinates of the vertices of the irregular quadrilateral element are (0,0,0), (30,8,0), (13,15,0), (9,15,0).

Figs. 13–30 show the subdivision results of these different elements with various source point locations. The source points are located close

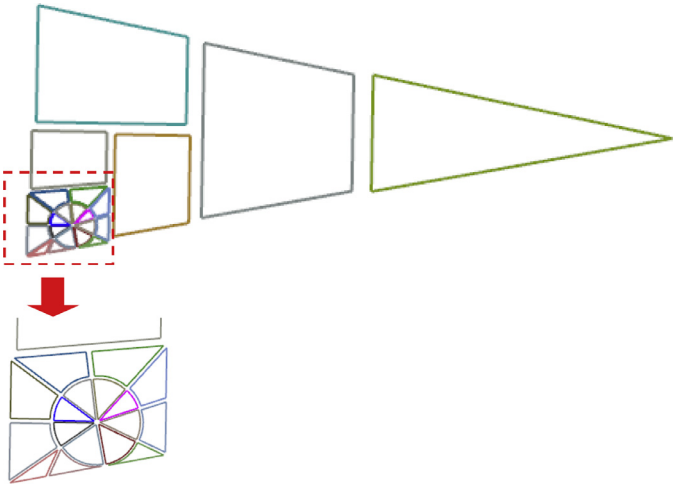

Fig. 16. Subdivision of slender triangular element with BTSM with source point at (0.09, 0.07).

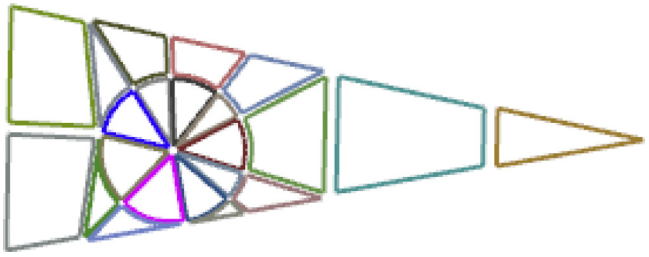

Fig. 17. Subdivision of slender triangular element with BTSM with source point at (0.295, 0.26).

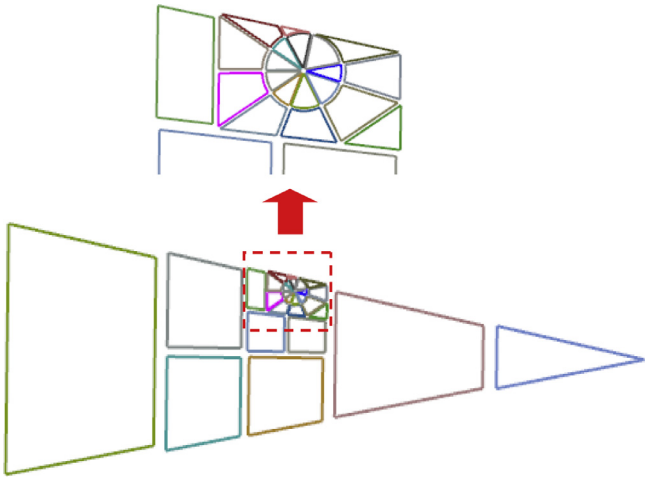

Fig. 18. Subdivision of slender triangular element with BTSM with source point at (0.5, 0.45).

to the vertices, close to the edges, or close to the center of the element. It can be seen from these figures that the shape of the resulting triangular singular patches around the source point are always regular, while the resulting non-singular patches close to the source point are smaller than those far away from the source point. Tables 2–19 show the accuracy obtained by the Binary Tree Subdivision Method (BTSM) and the Conventional Subdivision Method (CSM) in [30] for the different cases with different numbers of Gaussian quadrature points. It can be seen from the results shown in these tables that the BTSM renders the same level of accuracy as the CSM with much fewer quadrature points and thus, considerably increases the computational efficiency. In addition, significantly better accuracy is rendered by the BTSM than by the CSM for the same number of Gaussian quadrature points, consistently obtaining 2–4 orders of magnitude lower errors.

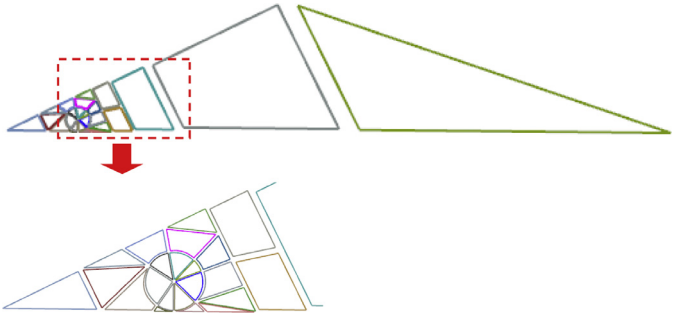

Fig. 19. Subdivision of obtuse triangular element with BTSM with source point at (0.09, 0.07).

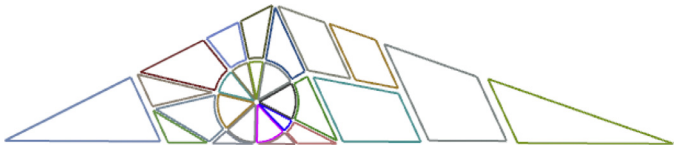

Fig. 20. Subdivision of obtuse triangular element with BTSM with source point at (0.295, 0.26).

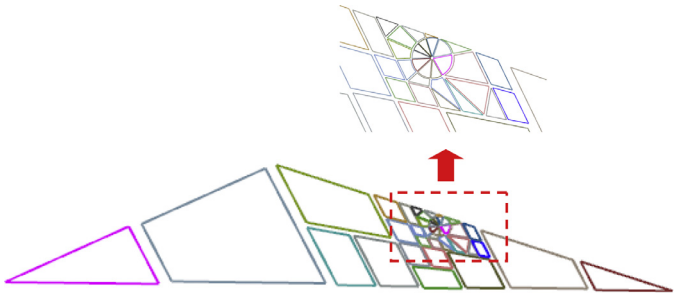

Fig. 21. Subdivision of obtuse triangular element with BTSM with source point at (0.5, 0.45).

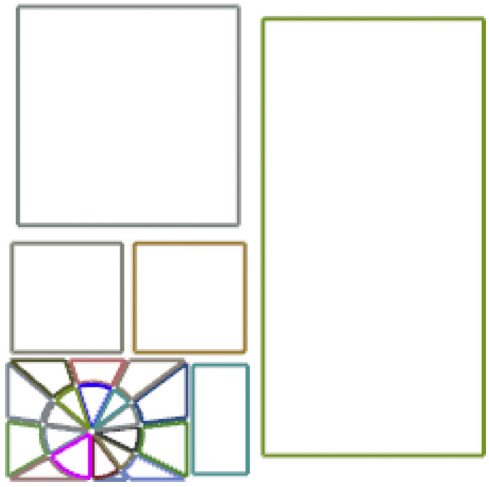

Fig. 22. Subdivision of regular quadrilateral element with BTSM with source point at (−0.65, −0.8).

Fig. 23. Subdivision of regular quadrilateral element with BTSM with source point at (0.075, −0.4).

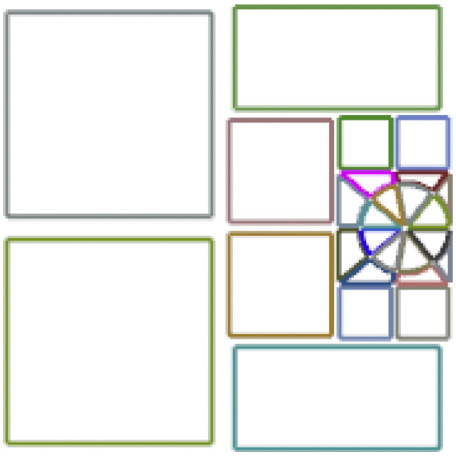

Fig. 24. Subdivision of regular quadrilateral element with BTSM with source point at (0.8, 0).

Fig. 25. Subdivision of slender quadrilateral element with BTSM with source point at (−0.85, −0.65).

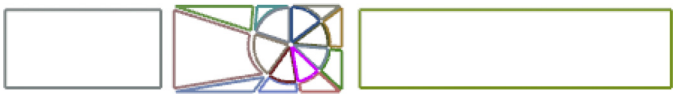

Fig. 26. Subdivision of slender quadrilateral element with BTSM with source point at (−0.15, 0.1).

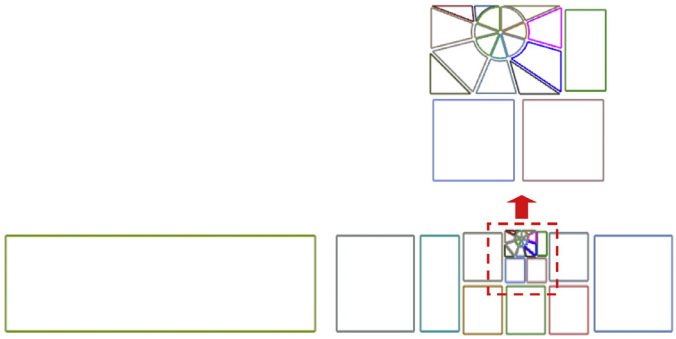

Fig. 27. Subdivision of slender quadrilateral element with BTSM with source point at (0.55, 0.85).

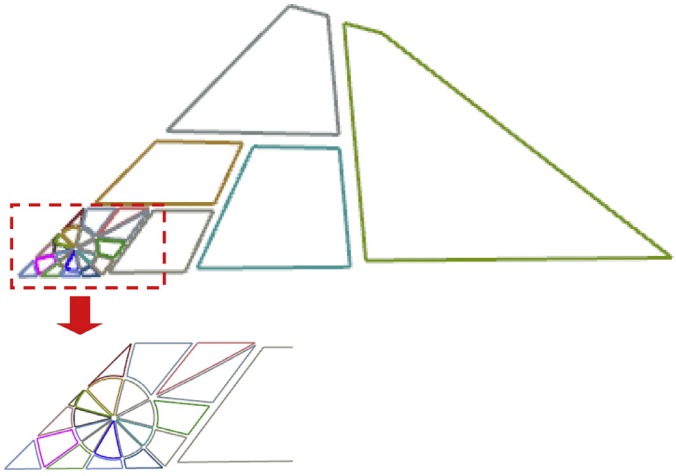

Fig. 28. Subdivision of irregular quadrilateral element with BTSM with source point at (−0.9, −0.8).

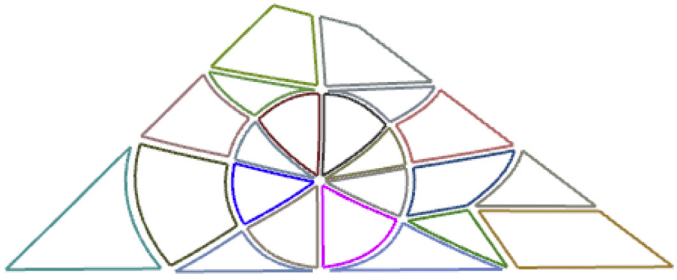

Fig. 29. Subdivision of irregular quadrilateral element with BTSM with source point at (−0.05, −0.3).

4.2. Singular integration on curved surface element examples

Curved surface elements with regular, slender, and obtuse triangular shapes are included in the following set of numerical experiments. The coordinates of the vertices of the regular triangular element are (0,0,0), (10,0,0), (5,8.6,0) while the midpoint coordinates of its edges are (5,0,1.5), (7.5,4.3,1.5), (2.5,4.3,1.5). The coordinates of the vertices of the slender triangular element are (0,0,0), (6,0,0), (3,15,0) while the midpoint coordinates of its edges are (3,0,1.5), (4.5,7.5,1.5), (1.5,7.5,1.5). The coordinates of the vertices of the obtuse triangular element are (0,0,0), (10,0,0), (20,10,0) while the midpoint coordinates of its edges are (5,0,1.5), (15,5,1.5), (10,5,1.5). In addition, curved quadrilateral elements are considered with regular, slender, and irregular shapes. The coordinates of the vertices of the regular quadrilateral element are (0,0,0), (10,0,0), (10,10,0), (0,10,0) while midpoint coordinates of its edges are (5,0,1.5), (10,5,1.5), (5,10,1.5), (0,5,1.5). The coordinates of the vertices of the slender quadrilateral element are (0,0,0), (20,0,0), (20,2.5,0), (0,2.5,0) while the midpoint coordinates of its edges are (10,0,2.0), (10,1.25,0.5), (10,2.5,2), (0,1.25,0.5). The coordinates of the vertices of the irregular quadrilateral element are (0,0,0),

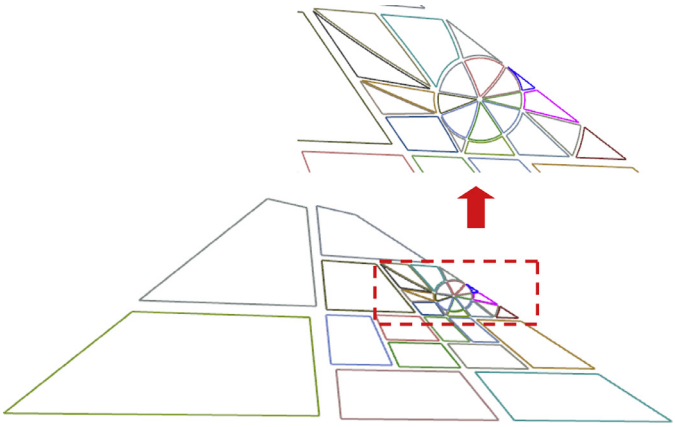

Fig. 30. Subdivision of irregular quadrilateral element with BTSM with source point at (0.8, 0.2).

Table 2
Numerical evaluation of weakly singular integral for regular triangular element with source point at (0.09, 0.07).

Planar element	Source point	Gaussian points number		Relative error	
		CSM	BTSM	CSM	BTSM
Regular triangular element	(0.09, 0.07)	121	121	2.9554e−003	2.2599e−004
		174	174	1.2358e−002	5.0567e−005
		307	307	5.3495e−004	9.7365e−006
		481	481	4.4043e−004	5.5284e−006
		583	583	8.1287e−004	3.4203e−008
		809	809	1.6742e−004	6.1972e−008

Table 3
Numerical evaluation of weakly singular integral for regular triangular element with source point at (0.295, 0.26).

Planar element	Source point	Gaussian points number		Relative error	
		CSM	BTSM	CSM	BTSM
Regular triangular element	(0.295, 0.26)	83	83	1.0606e−003	5.7159e−004
		115	115	8.3133e−004	9.5745e−005
		202	202	2.2135e−004	3.2915e−006
		327	327	3.7569e−005	8.2099e−007
		380	380	1.3330e−005	4.8382e−007
		552	552	8.6668e−007	1.4160e−009

Table 4
Numerical evaluation of weakly singular integral for regular triangular element with source point at (0.5, 0.45).

Planar element	Source point	Gaussian points number		Relative error	
		CSM	BTSM	CSM	BTSM
Regular triangular element	(0.5, 0.45)	152	152	1.8260e−002	1.3805e−003
		249	249	8.5429e−003	3.3162e−005
		440	440	3.3110e−003	3.3153e−007
		661	661	1.0954e−003	4.6411e−007
		863	863	5.1375e−005	5.4615e−008
		1139	1139	7.3763e−004	5.1324e−009

(30,8,0), (13,15,0), (9,15,0) while the midpoint coordinates of its edges are (15,4,2), (21.5,11.5,1.5), (11,15,0.5), (4.5,7.5,1).

Figs. 31–48 show the resulting patches from the implementation of the BTSM on different curved elements with different locations of the source point. Tables 20–37 show the comparisons of the accuracy of the BTSM and the CSM for the different cases with various numbers of integration quadrature points. It can be seen from the results shown in these tables that the BTSM renders the same level of accuracy as the CSM with much fewer quadrature points and thus, considerably increases the computational efficiency. In addition, significantly better accuracy is rendered by the BTSM than by the CSM for the same number of Gaussian quadrature points, consistently obtaining 2–4 orders of magnitude lower

Table 5
Numerical evaluation of weakly singular integral for slender triangular element with source point at (0.09, 0.07).

Planar element	Source point	Gaussian points number		Relative error	
		CSM	BTSM	CSM	BTSM
Slender triangular element	(0.09, 0.07)	104	104	8.3591e−003	1.2209e−003
		166	166	1.0946e−002	6.1225e−005
		275	275	9.5531e−003	3.5923e−006
		418	418	3.3221e−003	1.0460e−006
		524	524	3.6074e−004	1.0535e−007
		707	707	1.2713e−003	9.2137e−010

Table 6
Numerical evaluation of weakly singular integral for slender triangular element with source point at (0.295, 0.26).

Planar element	Source point	Gaussian points number		Relative error	
		CSM	BTSM	CSM	BTSM
Slender triangular element	(0.295, 0.26)	93	93	2.5543e−003	4.7971e−004
		146	146	7.6259e−003	1.3992e−004
		226	226	1.8620e−003	3.8392e−006
		371	371	5.2480e−004	4.2577e−007
		441	441	7.4820e−005	1.6567e−007
		639	639	1.1466e−004	7.8371e−009

Table 7
Numerical evaluation of weakly singular integral for slender triangular element with source point at (0.5, 0.45).

Planar element	Source point	Gaussian points number		Relative error	
		CSM	BTSM	CSM	BTSM
Slender triangular element	(0.5,0.45)	138	138	3.4058e−002	1.5526e−003
		226	226	1.5573e−002	4.5253e−005
		393	393	1.8811e−002	1.0118e−005
		581	581	1.8507e−002	2.0119e−006
		727	727	1.6868e−002	3.0687e−007
		997	997	1.7491e−002	4.1289e−008

Table 8
Numerical evaluation of weakly singular integral for obtuse triangular element with source point at (0.09, 0.07).

Planar element	Source point	Gaussian points number		Relative Error	
		CSM	BTSM	CSM	BTSM
Obtuse triangular element	(0.09, 0.07)	114	114	5.9365e−002	7.2317e−004
		159	159	1.0288e−002	1.0811e−004
		255	255	1.6167e−002	1.6749e−005
		429	429	1.2240e−002	6.5579e−007
		527	527	1.7312e−002	8.9874e−007
		699	699	1.5619e−002	3.6610e−008

Table 9
Numerical evaluation of weakly singular integral for obtuse triangular element with source point at (0.295, 0.26).

Planar element	Source point	Gaussian points number		Relative error	
		CSM	BTSM	CSM	BTSM
Obtuse triangular element	(0.295, 0.26)	111	111	5.6448e−002	1.9808e−003
		149	149	2.8648e−002	1.7217e−005
		272	272	2.8313e−003	1.5048e−005
		429	429	8.7339e−003	8.6886e−007
		521	521	6.1167e−003	8.3253e−008
		720	720	9.5802e−004	3.5450e−008

Table 10
Numerical evaluation of weakly singular integral for obtuse triangular element with source point at (0.5, 0.45).

Planar element	Source point	Gaussian points number		Relative error	
		CSM	BTSM	CSM	BTSM
Obtuse triangular element	(0.5, 0.45)	181	181	3.4905e−002	2.8116e−003
		311	311	3.8567e−002	4.3414e−005
		521	521	1.3142e−002	1.8923e−005
		770	770	4.6304e−003	1.8939e−006
		1009	1009	7.8917e−003	2.6670e−007
		1359	1359	7.9906e−003	4.3442e−008

Table 11
Numerical evaluation of weakly singular integral for regular quadrilateral element with source point at (−0.65, −0.8).

Planar element	Source point	Gaussian points number		Relative error	
		CSM	BTSM	CSM	BTSM
Regular quadrilateral element	(−0.65, −0.8)	114	114	3.1124e−003	2.2658e−003
		178	178	1.4993e−003	2.5222e−004
		298	298	6.3035e−004	3.2881e−005
		467	467	4.2518e−005	3.3769e−005
		556	556	6.1780e−005	9.3626e−006
		800	800	1.3322e−005	1.5542e−007

Table 12
Numerical evaluation of weakly singular integral for regular quadrilateral element with source point at (0.075, −0.4).

Planar element	Source point	Gaussian points number		Relative error	
		CSM	BTSM	CSM	BTSM
Regular quadrilateral element	(0.075, −0.4)	66	66	8.7049e−004	1.8037e−004
		95	95	2.3845e−004	2.2842e−004
		173	173	1.7285e−005	5.7793e−006
		272	272	9.9491e−007	4.7952e−007
		311	311	1.9942e−007	2.0338e−007
		435	435	1.6194e−009	4.7704e−009

Table 13
Numerical evaluation of weakly singular integral for regular quadrilateral element with source point at (0.8, 0).

Planar element	Source point	Gaussian points number		Relative error	
		CSM	BTSM	CSM	BTSM
Regular quadrilateral element	(0.8, 0)	128	128	7.2627e−003	8.1976e−004
		224	224	2.9783e−003	4.0382e−005
		342	342	1.2338e−003	3.3562e−006
		518	518	3.3706e−004	4.6926e−007
		692	692	1.4222e−004	6.0312e−008
		974	974	3.9562e−005	2.0900e−009

Table 14
Numerical evaluation of weakly singular integral for slender quadrilateral element with source point at (−0.85, −0.65).

Planar element	Source point	Gaussian points number		Relative error	
		CSM	BTSM	CSM	BTSM
Slender quadrilateral element	(−0.85, −0.65)	116	116	3.7711e−002	1.8897e−003
		189	189	2.6009e−002	1.0769e−004
		322	322	1.2658e−002	7.3446e−006
		489	489	1.1563e−002	1.1969e−006
		633	633	4.4301e−003	2.3463e−007
		860	860	1.5331e−003	5.1433e−008

errors. This again reveals the superior accuracy and efficiency of the BTSM.

Table 15
Numerical evaluation of weakly singular integral for slender quadrilateral element with source point at (−0.15, 0.1).

Planar element	Source point	Gaussian points number		Relative error	
		CSM	BTSM	CSM	BTSM
Slender quadrilateral element	(−0.15, 0.1)	80	80	3.0759e−002	3.6039e−003
		146	146	2.1951e−002	1.8687e−004
		248	248	3.4275e−002	3.1158e−007
		374	374	1.9701e−002	3.4906e−006
		456	456	1.3560e−002	6.0455e−007
		629	629	3.3047e−003	5.7947e−008

Table 16
Numerical evaluation of weakly singular integral for slender quadrilateral element with source point at (0.55, 0.85).

Planar element	Source point	Gaussian points number		Relative error	
		CSM	BTSM	CSM	BTSM
Slender quadrilateral element	(0.55, 0.85)	154	154	3.9616e−002	1.8150e−003
		251	251	1.8154e−002	9.3401e−005
		432	432	1.1439e−003	3.8787e−006
		642	642	8.2489e−005	4.4343e−007
		835	835	2.1319e−002	8.6048e−008
		1107	1107	1.6300e−002	6.9535e−010

Table 17
Numerical evaluation of weakly singular integral for irregular quadrilateral element with source point at (−0.9, −0.8).

Planar element	Source point	Gaussian points number		Relative error	
		CSM	BTSM	CSM	BTSM
Irregular quadrilateral element	(−0.9, −0.8)	116	116	5.8955e−003	1.0698e−003
		179	179	2.9393e−003	2.9169e−004
		297	297	6.3554e−003	2.7556e−005
		463	463	2.2144e−003	3.3547e−006
		565	565	2.3807e−003	5.5267e−007
		776	776	1.1722e−003	2.6225e−007

Table 18
Numerical evaluation of weakly singular integral for irregular quadrilateral element with source point at (−0.05, −0.3).

Planar element	Source point	Gaussian points number		Relative error	
		CSM	BTSM	CSM	BTSM
Irregular quadrilateral element	(−0.05, −0.3)	93	93	6.5975e−003	2.4512e−004
		130	130	3.0132e−003	2.3295e−004
		223	223	6.2045e−004	1.5975e−006
		353	353	1.0993e−004	8.8173e−007
		429	429	4.0138e−005	3.2385e−007
		593	593	2.6716e−006	4.9413e−008

Table 19
Numerical evaluation of weakly singular integral for irregular quadrilateral element with source point at (0.8, 0.2).

Planar element	Source point	Gaussian points number		Relative error	
		CSM	BTSM	CSM	BTSM
Irregular quadrilateral element	(0.8, 0.2)	176	176	2.1217e−003	1.3477e−003
		290	290	9.5892e−003	1.1017e−004
		494	494	1.8893e−003	6.0678e−006
		736	736	1.0694e−003	2.1941e−006
		953	953	7.8915e−004	5.2146e−007
		1251	1251	1.9735e−004	2.6034e−007

4.3. Singular integration for the case with source point on an element's edge or vertex

In this part, the subdivision results of BTSM and corresponding numerical results are presented for the case with source point on an element's edge or vertex. The coordinates of the vertexes of planer slender quadrilateral element are (0, 0, 0), (20, 0, 0), (20, 2.5, 0), (0, 2.5,

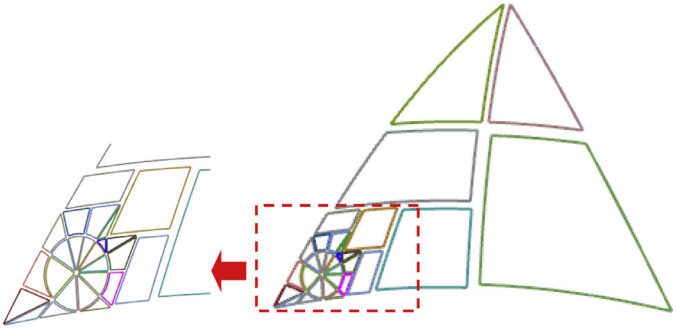

Fig. 31. Subdivision of curved regular triangular element with BTSM with source point at (0.09, 0.07).

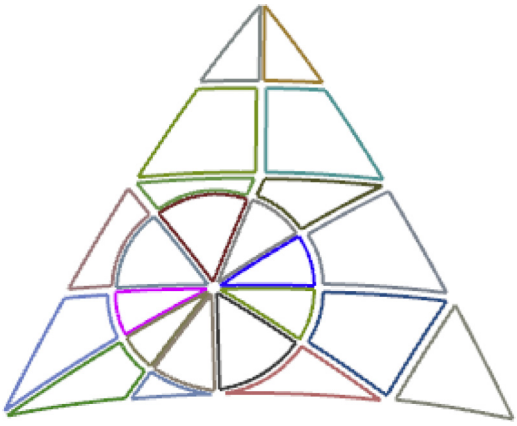

Fig. 32. Subdivision of curved regular triangular element with BTSM with source point at (0.295, 0.26).

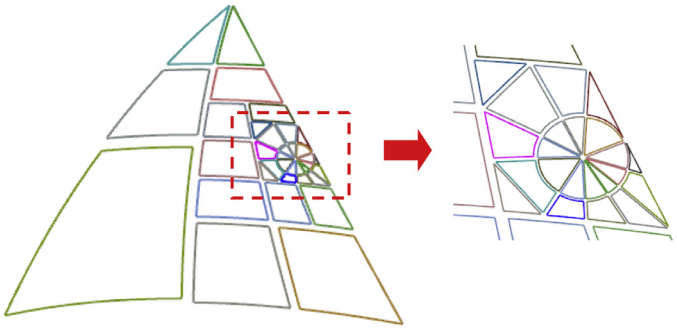

Fig. 33. Subdivision of curved regular triangular element with BTSM with source point at (0.5, 0.45).

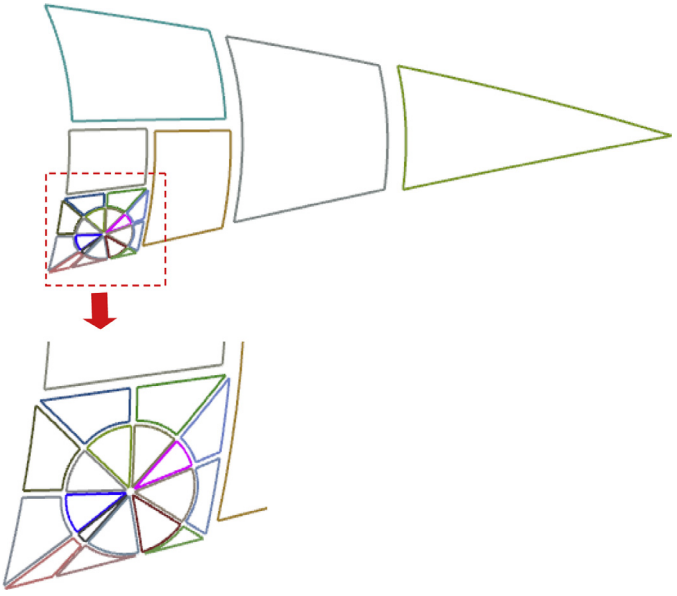

Fig. 34. Subdivision of curved slender triangular element with BTSM with source point at (0.09, 0.07).

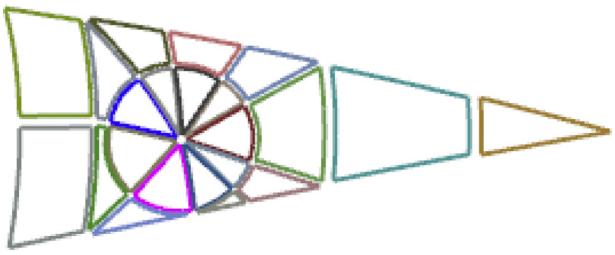

Fig. 35. Subdivision of curved slender triangular element with BTSM with source point at (0.295, 0.26).

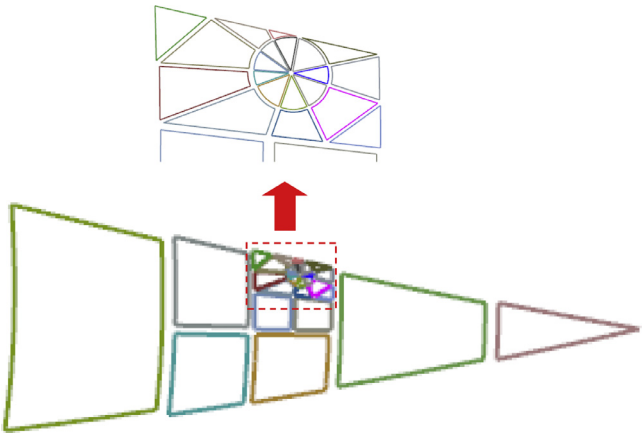

Fig. 36. Subdivision of curved slender triangular element with BTSM with source point at (0.5, 0.45).

0) in the physical coordinate system. The coordinates of the vertices of curved slender quadrilateral element are (0,0,0), (10,0,0), (10,10,0), (0,10,0) while midpoint coordinates of its edges are (5,0,1.5), (10,5,1.5), (5,10,1.5), (0,5,1.5). Figs. 49–51 show the element subdivision results for the case which source point is located on the element's vertex. The coordinate of this source point is (−1.0, −1.0) in the local coordinate system of the element. Figs. 50 and 52 show the element subdivision results for the case which source point is located on the element's edge. The coordinate of this source point is (−0.2, −1.0). It can be seen from these figures that the shape of the resulting triangular singular patches around the source point are always regular, while the resulting non-singular patches close to the source point are smaller than those far away from the source point.

Tables 38–41 show the comparisons of the accuracy of the BTSM and the CSM for the different cases with various numbers of integration quadrature points. It is seen that when the number of Gaussian quadrature points used is the same, the accuracy obtained by our method is 2–4

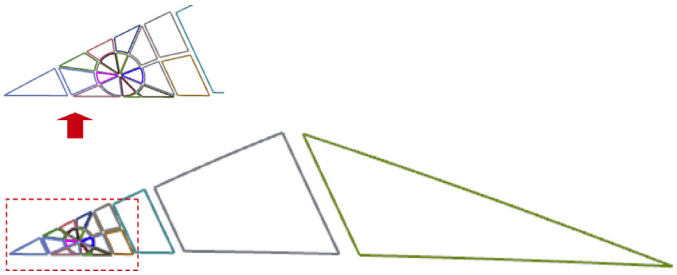

Fig. 37. Subdivision of curved obtuse triangular element with BTSM with source point at (0.09, 0.07).

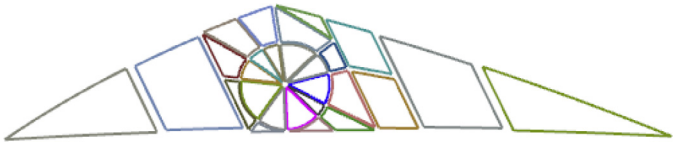

Fig. 38. Subdivision of curved obtuse triangular element with BTSM with source point at (0.32, 0.3).

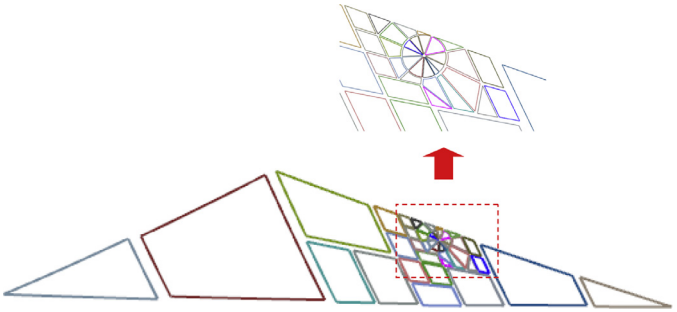

Fig. 39. Subdivision of curved obtuse triangular element with BTSM with source point at (0.5, 0.45).

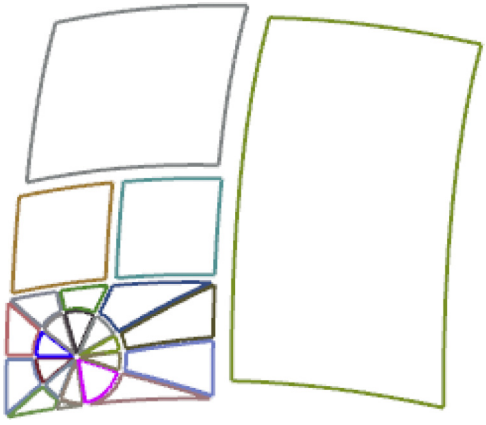

Fig. 40. Subdivision of curved regular quadrilateral element with BTSM with source point at (−0.65, −0.8).

orders of magnitude higher than that by the conventional method. On the other hand, the BTSM renders the same level of accuracy as the CSM with much fewer quadrature points and thus, considerably increases the computational efficiency. The effectiveness and accuracy of our method are demonstrated again.

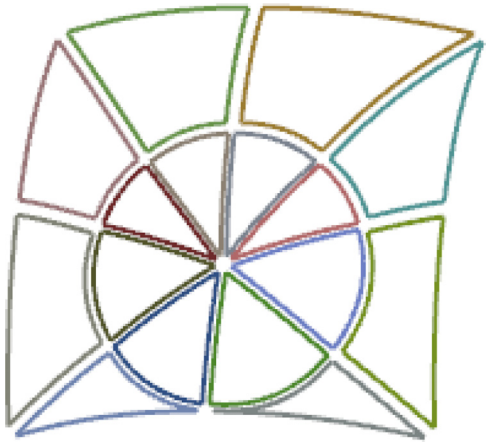

Fig. 41. Subdivision of curved regular quadrilateral element with BTSM with source point at (0.075, −0.4).

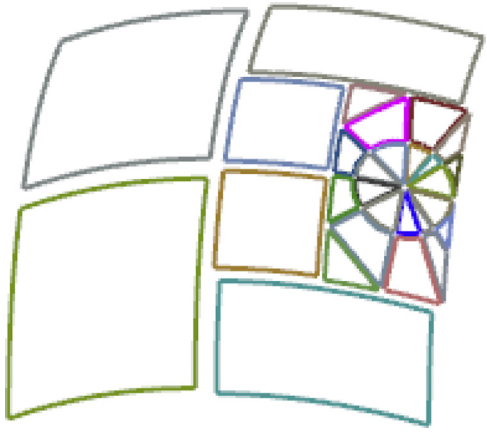

Fig. 42. Subdivision of curved regular quadrilateral element with BTSM with source point at (0.8, 0).

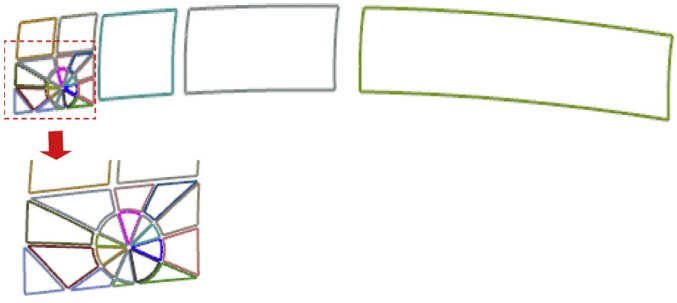

Fig. 43. Subdivision of curved slender quadrilateral element with BTSM with source point at (−0.85, −0.65).

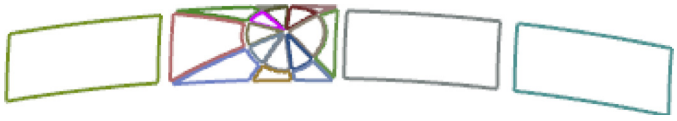

Fig. 44. Subdivision of curved slender quadrilateral element with BTSM with source point at (−0.15, 0.1).

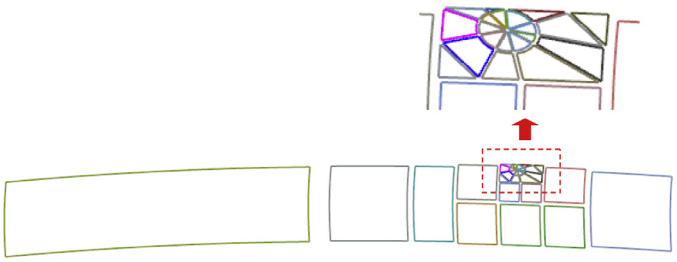

Fig. 45. Subdivision of curved slender quadrilateral element with BTSM with source point at (0.55, 0.85).

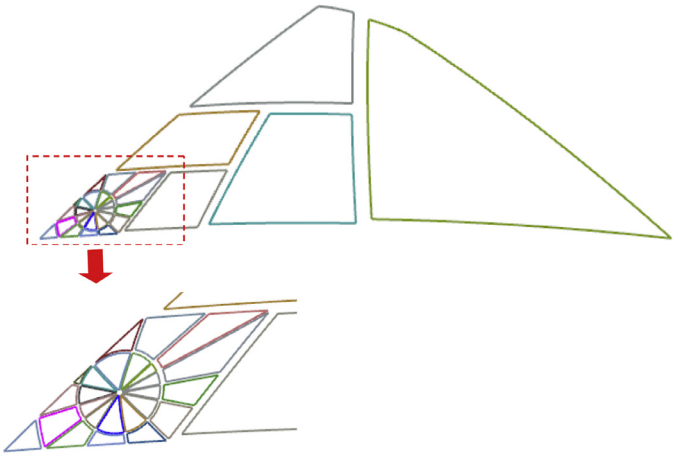

Fig. 46. Subdivision of curved irregular quadrilateral element with BTSM with source point at (−0.9, −0.8).

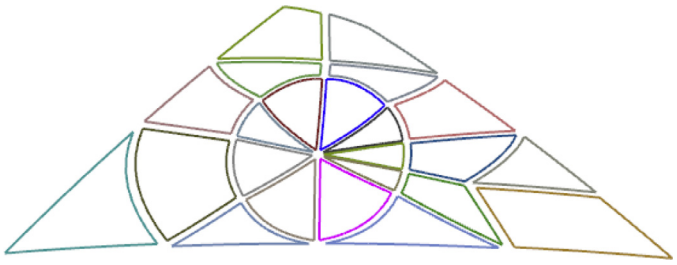

Fig. 47. Subdivision of curved irregular quadrilateral element with BTSM with source point at (−0.05, −0.3).

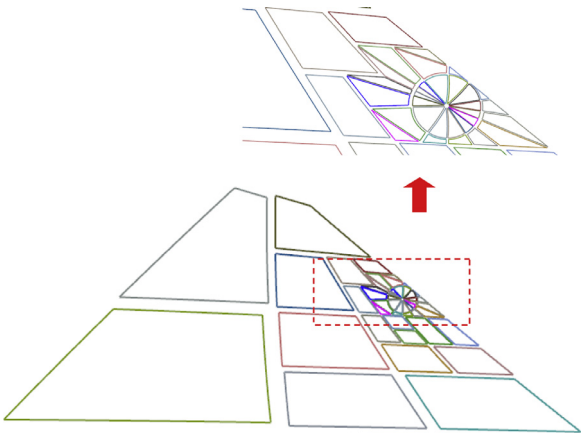

Fig. 48. Subdivision of curved irregular quadrilateral element with BTSM with source point at (0.85, 0.15).

Fig. 49. Subdivision of slender quadrilateral element with BTSM with source point at (−1.0, −1.0).

Fig. 50. Subdivision of slender quadrilateral element with BTSM with source point at (−0.2, −1.0).

Fig. 51. Subdivision of curved slender quadrilateral element with BTSM with source point at (−1.0, −1.0).

Fig. 52. Subdivision of curved slender quadrilateral element with BTSM with source point at (−0.2, −1.0).

Table 20
Numerical evaluation of weakly singular integral for curved regular triangular element with source point at (0.09, 0.07).

Curved surface element	Source point	Gaussian points number		Relative error	
		CSM	BTSM	CSM	BTSM
Regular triangular element	(0.09, 0.07)	143	143	8.0612e−003	4.6274e−004
		205	205	3.0986e−003	4.5356e−005
		353	353	6.2135e−004	1.5576e−005
		541	541	1.3612e−003	4.5272e−006
		663	663	7.8584e−005	4.3965e−007
		932	932	2.8893e−004	5.0738e−008

Table 21
Numerical evaluation of weakly singular integral for curved regular triangular element with source point at (0.295, 0.26).

Curved surface element	Source point	Gaussian points number		Relative error	
		CSM	BTSM	CSM	BTSM
Regular triangular element	(0.295, 0.26)	86	86	9.7433e−004	1.1619e−003
		129	129	7.8937e−004	1.2817e−004
		223	223	2.1635e−004	8.1441e−007
		333	333	3.8047e−005	8.5297e−007
		421	421	1.3933e−005	1.1129e−007
		589	589	9.6327e−008	1.8139e−008

Table 22
Numerical evaluation of weakly singular integral for curved regular triangular element with source point at (0.5, 0.45).

Curved surface element	Source point	Gaussian points number		Relative error	
		CSM	BTSM	CSM	BTSM
Regular triangular element	(0.5, 0.45)	154	154	1.7525e−002	1.3827e−003
		255	255	8.2126e−003	3.4470e−005
		458	458	3.0808e−003	9.0581e−007
		680	680	9.7590e−005	2.4965e−007
		900	900	4.1079e−004	4.8255e−008
		1209	1209	5.6274e−004	1.0528e−009

Table 23
Numerical evaluation of weakly singular integral for curved slender triangular element with source point at (0.09, 0.07).

Curved surface element	Source point	Gaussian points number		Relative error	
		CSM	BTSM	CSM	BTSM
Slender triangular element	(0.09, 0.07)	106	106	1.5319e−002	1.6260e−003
		156	156	5.1578e−003	7.2125e−005
		280	280	6.5965e−003	1.4435e−006
		425	425	3.7297e−003	1.2479e−006
		523	523	1.2545e−003	2.5723e−007
		722	722	5.2032e−005	3.7627e−008

Table 24
Numerical evaluation of weakly singular integral for curved slender triangular element with source point at (0.295, 0.26).

Curved surface element	Source point	Gaussian points number		Relative error	
		CSM	BTSM	CSM	BTSM
Slender triangular element	(0.295, 0.26)	85	85	3.4374e−003	1.5020e−003
		136	136	6.8870e−003	1.2916e−004
		221	221	2.0174e−003	3.5759e−006
		352	352	8.0888e−004	8.2836e−007
		435	435	1.2003e−004	1.8088e−007
		618	618	9.7663e−005	3.5017e−009

Table 25
Numerical evaluation of weakly singular integral for curved slender triangular element with source point at (0.5, 0.45).

Curved surface element	Source point	Gaussian points number		Relative error	
		CSM	BTSM	CSM	BTSM
Slender triangular element	(0.5, 0.45)	130	130	3.2247e−002	1.7953e−003
		222	222	1.3967e−002	7.3229e−005
		375	375	1.7248e−002	9.8854e−006
		582	582	1.6914e−002	1.8463e−006
		746	746	1.5275e−002	2.8591e−007
		995	995	1.4889e−002	4.5124e−008

Table 26
Numerical evaluation of weakly singular integral for curved obtuse triangular element with source point at (0.09, 0.07).

Curved surface element	Source point	Gaussian points number		Relative error	
		CSM	BTSM	CSM	BTSM
Obtuse triangular element	(0.09, 0.07)	112	112	4.9220e−002	4.2084e−004
		160	160	1.7505e−002	4.2046e−005
		268	268	1.5665e−002	1.1319e−005
		435	435	2.4636e−002	3.6368e−006
		526	526	9.7278e−003	6.4204e−007
		736	736	1.1534e−002	1.3255e−007

Table 27
Numerical evaluation of weakly singular integral for curved obtuse triangular element with source point at (0.32, 0.3).

Curved surface element	Source point	Gaussian points number		Relative error	
		CSM	BTSM	CSM	BTSM
Obtuse triangular element	(0.32, 0.3)	116	116	7.0254e−003	1.2737e−003
		152	152	1.7592e−002	3.7817e−005
		277	277	1.4307e−002	3.1764e−007
		440	440	6.1355e−003	3.9105e−007
		520	520	3.7094e−003	2.3373e−007
		721	721	8.2447e−004	2.8962e−009

Table 28
Numerical evaluation of weakly singular integral for curved obtuse triangular element with source point at (0.5, 0.45).

Curved surface element	Source point	Gaussian points number		Relative error	
		CSM	BTSM	CSM	BTSM
Obtuse triangular element	(0.5, 0.45)	186	186	3.2191e−002	2.9247e−003
		312	312	3.3532e−002	8.2714e−005
		519	519	1.1695e−002	1.7367e−005
		803	803	3.6133e−003	3.0716e−006
		1013	1013	6.5561e−003	2.3877e−006
		1382	1382	6.4658e−003	1.9805e−007

Table 29
Numerical evaluation of weakly singular integral for curved regular quadrilateral element with source point at (−0.65, −0.8).

Curved surface element	Source point	Gaussian points number		Relative error	
		CSM	BTSM	CSM	BTSM
Regular quadrilateral element	(−0.65, −0.8)	107	107	4.9580e−003	2.4608e−003
		167	167	2.1057e−003	7.8087e−005
		291	291	6.4295e−004	6.1722e−005
		445	445	1.2922e−004	6.2385e−005
		558	558	1.1589e−006	1.1187e−007
		773	773	9.9754e−006	1.6716e−006

Table 30
Numerical evaluation of weakly singular integral for curved regular quadrilateral element with source point at (0.075, −0.4).

Curved surface element	Source point	Gaussian points number		Relative error	
		CSM	BTSM	CSM	BTSM
Regular quadrilateral element	(0.075, −0.4)	64	64	7.3413e−004	7.8176e−004
		94	94	2.0210e−004	2.2118e−004
		169	169	1.5208e−005	6.1768e−007
		266	266	9.5818e−007	5.6834e−007
		315	315	2.1706e−007	2.8309e−007
		437	437	6.4614e−009	8.0229e−009

Table 31
Numerical evaluation of weakly singular integral for curved regular quadrilateral element with source point at (0.8, 0).

Curved surface element	Source point	Gaussian points number		Relative error	
		CSM	BTSM	CSM	BTSM
Regular quadrilateral element	(0.8, 0)	136	136	5.5627e−003	5.6649e−004
		200	200	2.0871e−003	2.7523e−005
		338	338	7.9274e−004	2.2014e−006
		526	526	1.9007e−004	1.1246e−007
		648	648	1.1803e−004	2.5139e−008
		880	880	2.8925e−005	3.1386e−009

Table 32
Numerical evaluation of weakly singular integral for curved slender quadrilateral element with source point at (−0.85, −0.65).

Curved surface element	Source point	Gaussian points number		Relative error	
		CSM	BTSM	CSM	BTSM
Slender quadrilateral element	(−0.85, −0.65)	136	136	5.5627e−003	5.6649e−004
		200	200	2.0871e−003	2.7523e−005
		338	338	7.9274e−004	2.2014e−006
		526	526	1.9007e−004	1.1246e−007
		648	648	1.1803e−004	2.5139e−008
		880	880	2.8925e−005	3.1386e−009

Table 33
Numerical evaluation of weakly singular integral for curved slender quadrilateral element with source point at (−0.15, 0.1).

Curved surface element	Source point	Gaussian points number		Relative error	
		CSM	BTSM	CSM	BTSM
Slender quadrilateral element	(−0.15, 0.1)	92	92	2.7635e−002	8.2666e−004
		149	149	4.1450e−002	1.9373e−004
		258	258	3.2439e−002	1.5678e−005
		397	397	1.8694e−002	3.9971e−006
		500	500	1.2962e−002	8.0560e−007
		666	666	3.3975e−003	1.7164e−007

Table 34
Numerical evaluation of weakly singular integral for curved slender quadrilateral element with source point at (0.55, 0.85).

Curved surface element	Source point	Gaussian points number		Relative error	
		CSM	BTSM	CSM	BTSM
Slender quadrilateral element	(0.55, 0.85)	92	92	2.7635e−002	8.2666e−004
		149	149	4.1450e−002	1.9373e−004
		258	258	3.2439e−002	1.5678e−005
		397	397	1.8694e−002	3.9971e−006
		500	500	1.2962e−002	8.0560e−007
		666	666	3.3975e−003	1.7164e−007

Table 35
Numerical evaluation of weakly singular integral for curved irregular quadrilateral element with source point at (−0.9, −0.8).

Curved surface element	Source point	Gaussian points number		Relative error	
		CSM	BTSM	CSM	BTSM
Irregular quadrilateral element	(−0.9, −0.8)	128	128	6.2513e−003	9.3862e−004
		191	191	3.6553e−003	3.2688e−004
		324	324	8.2585e−005	1.9926e−005
		522	522	2.6911e−003	2.1158e−006
		636	636	2.0560e−003	3.5802e−007
		893	893	5.1339e−005	2.2779e−008

Table 36
Numerical evaluation of weakly singular integral for curved irregular quadrilateral element with source point at (−0.05, −0.3).

Curved surface element	Source point	Gaussian points number		Relative error	
		CSM	BTSM	CSM	BTSM
Irregular quadrilateral element	(−0.05, −0.3)	91	91	6.5332e−003	1.3379e−003
		144	144	2.9859e−003	1.9298e−004
		237	237	6.1788e−004	2.1877e−005
		372	372	4.1316e−005	1.5415e−006
		461	461	1.2559e−005	1.8484e−007
		643	643	2.1701e−006	2.1529e−008

Table 37
Numerical evaluation of weakly singular integral for curved irregular quadrilateral element with source point at (0.85, 0.15).

Curved surface element	Source point	Gaussian points number		Relative error	
		CSM	BTSM	CSM	BTSM
Irregular quadrilateral element	(0.85, 0.15)	225	225	4.8066e−003	1.0839e−003
		356	356	5.4583e−003	6.8342e−005
		617	617	2.2752e−003	2.9372e−005
		924	924	1.7689e−003	6.5676e−007
		1214	1214	7.2703e−004	8.2396e−007
		1651	1651	4.9179e−004	1.4276e−008

Table 38
Numerical evaluation of weakly singular integral for slender quadrilateral element with source point at (−1.0, −1.0).

Planer element	Source point	Gaussian points number		Relative error	
		CSM	BTSM	CSM	BTSM
Slender quadrilateral element	(−1.0, −1.0)	40	40	1.2273e−002	4.1238e−004
		65	65	7.3064e−003	6.5700e−006
		93	93	1.2974e−003	1.3276e−006
		156	156	2.6414e−004	3.9609e−007
		212	212	6.3547e−005	2.9461e−008
		274	274	6.5187e−006	4.7085e−009

Table 39
Numerical evaluation of weakly singular integral for slender quadrilateral element with source point at (−0.2, −1.0).

Planer element	Source point	Gaussian points number		Relative error	
		CSM	BTSM	CSM	BTSM
Slender quadrilateral element	(−0.2, −1.0)	60	60	5.0483e−003	1.2742e−003
		96	96	1.6124e−002	6.5546e−005
		169	169	8.9751e−003	3.2485e−006
		257	257	2.6099e−003	5.4214e−007
		317	317	1.0470e−003	1.0661e−007
		449	449	8.3829e−005	1.0287e−008

Table 40
Numerical evaluation of weakly singular integral for curved slender quadrilateral element with source point at (−1.0, −1.0).

Curved surface element	Source point	Gaussian points number		Relative error	
		CSM	BTSM	CSM	BTSM
Slender quadrilateral element	(−1.0, −1.0)	48	48	5.5005e−003	4.3350e−004
		81	81	1.4076e−003	5.6162e−005
		120	120	1.6583e−004	6.1532e−006
		188	188	1.4512e−004	4.5261e−007
		243	243	7.3477e−006	1.0828e−007
		333	333	3.3446e−006	1.7679e−008

Table 41
Numerical evaluation of weakly singular integral for slender quadrilateral element with source point at (−0.2, −1.0).

Curved surface element	Source point	Gaussian points number		Relative error	
		CSM	BTSM	CSM	BTSM
Slender quadrilateral element	(−0.2, −1.0)	60	60	6.9829e−003	9.2268e−004
		99	99	1.3360e−002	2.0766e−004
		173	173	6.4195e−003	1.0490e−005
		266	266	1.5792e−003	4.2021e−007
		321	321	5.4755e−004	2.5478e−007
		470	470	9.6056e−005	1.4015e−008

5. Conclusions

A binary-tree subdivision method (BTSM) for the accurate and efficient evaluation of weakly singular integrals in three-dimensional (3D) Boundary Element Method (BEM) is formulated and implemented in this paper. When singular boundary elements are irregularly shaped or the source point is too close to its vertices or edges, the patches obtained by conventional subdivision methods usually yield low integration accuracy. In the BTSM the resulting subdivision patch distribution is dense close to the source point and sparse far from the source point, while the source point is isolated with a circular cavity that is subdivided using regular triangular elements converging on the source point. The resulting triangular patches around the source point are modeled using four-node serendipity where the outer arch is approximated using quadratic shape functions to yield constrained limits for direct standard Gaussian quadrature integration. This renders the BTSM highly computationally

efficient while ensuring high order accuracy. The BTSM is applicable to any regularly or irregularly shaped planar or curved element with arbitrary location of the source point. Numerical examples are presented for planar and curved elements with different shapes and various locations of the source point, demonstrating significant improvements in accuracy and efficiency when compared to conventional element subdivision methods.

Acknowledgments

This work was supported by National Science Foundation of China under grant numbers 11772125 and 11472102.

References

[1] Zhang J, Lu C, Zhang X, et al. An adaptive element subdivision method for evaluation of weakly singular integrals in 3D BEM. Eng Anal Bound Elem 2015;51:213–19.
[2] Zhang J, Wang P, Lu C, et al. A spherical element subdivision method for the numerical evaluation of nearly singular integrals in 3D BEM. Eng Comput 2017;34(6):2074–87.
[3] Zhang J, Lin W, Dong Y, et al. A double-layer interpolation method for implementation of BEM analysis of problems in potential theory. Appl Math Model 2017;51:250–69.
[4] Ma H, Kamiya N. Distance transformation for the numerical evaluation of near singular boundary integrals with various kernels in boundary element method. Eng Anal Bound Elem 2002;26(4):329–39.
[5] Liu YJ, Rudolphi TJ. Some identities for fundamental solutions and their applications to weakly-singular boundary element formulations. Eng Anal Bound Elem 1991;8:301–11.
[6] Zhong Y, Zhang J, Dong Y, et al. A serendipity triangular patch for evaluating weakly singular boundary integrals. Eng Anal Bound Elem 2016;69:86–92.
[7] Zhang Y, Li X, Sladek V, et al. A new method for numerical evaluation of nearly singular integrals over high-order geometry elements in 3D BEM. Elsevier Science Publishers B. V.; 2015.
[8] Gao X-W, Feng W-Z, Yang K, Cui M. Projection plane method for evaluation of arbitrary high order singular boundary integrals. Eng Anal Bound Elem 2014;50:265–74.
[9] Guiggiani M, Krishnasamy G, Rudolphi TJ, Rizzo FJ. A general algorithm for the numerical solution of hypersingular boundary integral equations. J Appl Mech 1992;59(3):604–14 Transactions ASME.
[10] Qu W, Zhang Y, Gu Y, et al. Three-dimensional thermal stress analysis using the indirect BEM in conjunction with the radial integration method. Adv Eng Softw 2017;112:147–53.
[11] Gao X-W, Zheng Y-T, Peng H-F, Cui M, Zhang Z-Y. Trans-accuracy elements and their application in BEM analysis of structurally multi-scale problems. Eng Anal Bound Elem 2018;97:82–93.
[12] Zhang Y, Gong Y, Gao X. Calculation of 2D nearly singular integrals over high--order geometry elements using the sinh transformation. Eng Anal Bound Elem 2015;60:144–53.
[13] Feng W-Z, Liu J, Gao X-W. An improved direct method for evaluating hypersingular stress boundary integral equations in BEM. Eng Anal Bound Elem 2015;61:274–81.
[14] Karami G, Derakhshan D. An efficient method to evaluate hypersingular and supersingular integrals in boundary integral equations analysis. Eng Anal Bound Elem 1999;23(4):317–26.
[15] Gao X-W. An effective method for numerical evaluation of general 2D and 3D high order singular boundary integrals. Comput Methods Appl Mech Eng 2010;199(45–48):2856–64.
[16] Cheng HD, Detournay E. On singular integral equations and fundamental solutions of poroelasticity. Int J Solids Struct 1998;35(34–35):4521–55.
[17] Niu Z, Wendland WL, Wang X, et al. A semi-analytical algorithm for the evaluation of the nearly singular integrals in three-dimensional boundary element methods. Comput Methods Appl Mech Eng 2005;194(9–11):1057–74.
[18] Zhang J, Han L, Lin W, et al. A new implementation of BEM by an expanding element interpolation method. Eng Anal Bound Elem 2017;78:1–7.
[19] Zhang Y. An kind of non-singular boundary integral method for plane potential problems. Pure Appl Math 2001;17(2):161–4.
[20] Klees R. Numerical calculation of weakly singular surface integrals. J Geod 1996;70(11):781–97.
[21] Divo E, Kassab AJ. Boundary element method for heat conduction: with applications in non-homogeneous media, topics in engineering series, 44. Billerica, MA: WIT Press; 2002.
[22] Pepper D, Kassab A, Divo E. An introduction to finite element, boundary element, and meshless methods: with applications to heat transfer and fluid flow. ASME Press; 2014.
[23] Zhang J, Qin X, Han X, et al. A boundary face method for potential problems in three dimensions. Int J Numer Methods Eng 2009;80(3):320–37.
[24] Tanaka M, Zhang JM, Matsumoto T. Boundary-type meshless solution of potential problems: comparison between singular and regular formulations in hybrid BNM. Trans JASCOME, J Bound Elem Methods 2003;20:21–6.
[25] Thompson JF, Soni BK, Weatherill NP. Handbook of grid generation 1998.
[26] Ooi ET, Man H, Natarajan S, et al. Adaptation of quadtree meshes in the scaled boundary finite element method for crack propagation modelling. Eng Fract Mech 2015;144:101–17.
[27] Dong Y, Zhang J, Xie G, et al. A general algorithm for the numerical evaluation of domain integrals in 3D boundary element method for transient heat conduction. Eng Anal Bound Elem 2015;51(3):30–6.
[28] Bu S, Davies TG. Effective evaluation of non-singular integrals in 3D BEM. Adv Eng Softw 1995;23(2):121–8.
[29] Lachat JC, Watson JO. Effective numerical treatment of boundary integral equations: a formulation for three-dimensional elastostatics. Int J Numer Methods Eng 2010;10(5):991–1005.
[30] Telles JCF. A self-adaptive co-ordinate transformation for efficient numerical evaluation of general boundary element integrals. Int J Numer Methods Eng 1987;24:959–73.